JOURNAL OF MATERIALS SCIENCE 3 (1968) 457–463

The Effect of Inclusions on the Stress Distribution in Solids

D. V. EDMONDS, C. J. BEEVERS
Department of Physical Metallurgy and Science of Materials, The University, Birmingham, UK

Received 5 March 1968

The stress distribution existing in and around hard inclusions in solids subjected to a uniaxially applied stress has been investigated. Two-dimensional models containing inclusions of various shapes and orientations have been analysed by means of the photoelasticity technique, and the influence of elastic modulus, shape, and orientation of inclusions on the stress concentrations produced has been examined further by a mathematical treatment.

1. Introduction

Many engineering materials contain second-phase inclusions whose presence is necessary for strengthening purposes. Frequently, however, inclusions exist solely as impurities, either legacies of the starting materials or manufacturing processes, or formed during use. The presence of these second phases should contribute towards the non-uniform distribution of an applied stress, and may result in severe stress concentrations and local plastic deformation.

Etch-pit studies of lithium fluoride [1] and silicon-iron [2] have clearly revealed dislocation generation at impurity inclusions. Bullen *et al* [3] have recently shown that discontinuous yielding in Armco iron can be eliminated, and the yield stress reduced by more than half, following subjection to hydrostatic pressure prior to testing. Moreover, recrystallised chromium, which is normally brittle at room temperature, showed good ductility ($\sim$ 60% strain) after pressurisation, and yielded at about half the fracture stress of non-pressurised chromium [4]. In both materials this behaviour has been explained by the creation of free dislocations at impurity inclusions during the pressurisation treatment. An investigation by McCarthy *et al* [5] of zinc composites containing spheroidal particles of ZnO, α-Al_2O_3 or tungsten, showed substantial dispersion-strengthening at elevated temperatures. At room temperature, however, the presence of the particles reduced the yield stress of the zinc by about half and increased the ductility. Again this behaviour can be attributed, at least in part, to the non-uniformity of stress introduced into the zinc by the presence of the second phase.

The perturbation of an otherwise uniform applied stress by an inclusion has been the subject of a number of mathematical analyses [6–10], and considerable progress towards an exact solution has been made. Nevertheless, the difficulties associated with the mathematical treatment of arbitrary inclusion shape have served to keep the problem academic. In 1938, however, Thibodeau and Wood [11] utilised the then relatively undeveloped photoelasticity technique of stress-analysis to determine the stress distribution around a rigid circular inclusion, and this experimental approach yielded results similar to theoretical studies. More recently, the photoelasticity technique has been adopted to analyse the shear stress distribution associated with the transfer of load from matrix to fibre in a fibre-reinforced composite [12–15].

The present paper reports the results of an investigation in which the effect of hard inclusions on local magnification of an applied stress was examined, both by a photoelasticity technique and by a theoretical analysis due to Eshelby [10].

2. Experimental

The properties of the materials used to construct

the photoelastic models used in the investigation are given in table I. Araldite CT200 is an epoxy resin plastic produced by Ciba (ARL) Ltd*, and sold in sheet form by Sharples Engineering Co Ltd†. Photostress is another epoxy resin marketed in sheet form by Budd S.A.‡

TABLE I Material properties.

Material	Modulus of elasticity ($\times 10^4$ kg/cm^2)	Material fringe constant (kg/cm fringe)
Brass	105†	Opaque
Araldite CT200	3.5‡	9.1§
Photostress A*	2.8-3.5‡	—
Photostress B*	0.2‡	—

*Designated A and B for purpose of this paper.
†From C. J. Smithells, "Metals Reference Book", Vol. II (Butterworths, 1962).
‡From manufacturers' data.
§Calibrated experimentally.

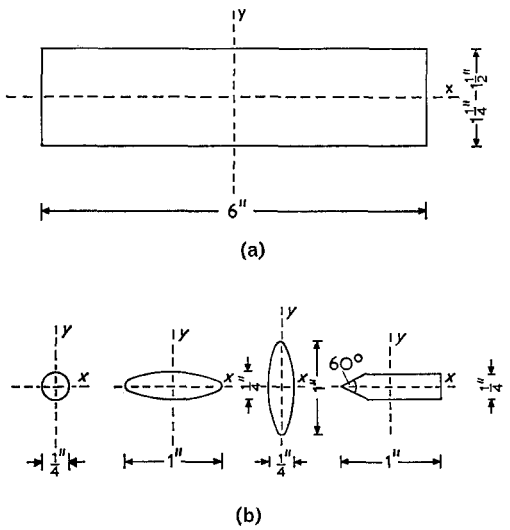

Figure 1 Dimensions of photoelastic models: (a) rectangular plate; (b) hole shapes. *Note* Inches are used in this diagram; 1.0 in. = 2.5 cm.

Rectangular plates having the dimensions illustrated by fig. 1a were machined from Araldite CT200 and Photostress B. Holes having the shapes and dimensions shown in fig. 1b were cut at the centres of the plates, their orientations being indicated in fig. 1 by the x and y axes. Inserts were machined from brass and Photostress A and cemented into the holes using Araldite adhesive.

The photoelastic models were loaded in uniaxial tension in a transmission polariscope, and the isochromatic and isoclinic fringe patterns recorded photographically. Direct observation of the fringe pattern through a travelling microscope also enabled the maximum fringe order and position of the fringes to be determined more accurately.

3. Results

Fig. 2 indicates the isoclinic fringe patterns and the principal stress trajectories constructed from them for circular and elliptical inclusions (Araldite/brass models). Typical isochromatic fringe patterns obtained in the Araldite/brass models are shown in fig. 3§. The isochromatic fringes developed in the region of the point at which the applied stress axis intercepts the inclusion boundary. With increasing applied stress, the fringes thus produced in the matrix at each end of the inclusion expanded outwards and joined up near the perimeter of the model, moving back towards the sides of the inclusions where they eventually disappeared. Only at the square end of the irregularly shaped inclusion (fig. 3d) could it be observed that the region of maximum fringe order occurred at a finite distance from the end of the inclusion; the fringes developed there separated, one part moving as described above whilst the other moved directly towards the inclusion and disappeared. Fig. 3e illustrates a case where the adhesion between the inclusion and the matrix failed at one end of the inclusion. The modified isochromatic fringe pattern produced at this end owing to the presence of the crack can be readily compared with the normal fringe pattern at the other end of the inclusion, thus demonstrating the importance of end adhesion to the stress distribution produced in the models.

Fig. 4 shows how the ratio of maximum shear stress in the plane of the model (τ) to applied normal stress (σ) varies as a function of distance from the inclusion along the applied stress axis, for various inclusion orientations and end shapes. The maximum shear stress is calculated from the photoelastic data, using the relationship [16]

$$\tau = (P - Q)/2 = Nf/2t \qquad (1)$$

*Address: Duxford, Cambridge, UK
†Address: Walton-le-Dale, Preston, UK
‡Address: Neuilly-sur-Seine, France
§Applied stress axis horizontal in all photographs.

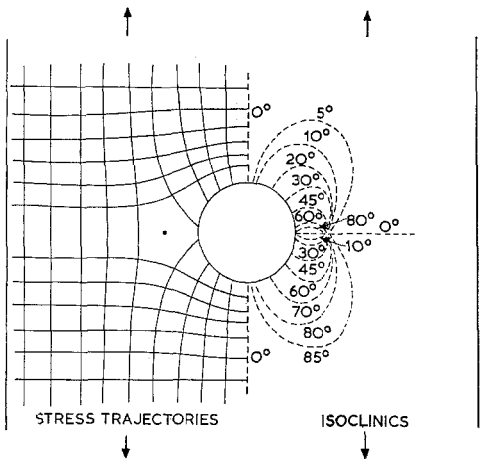

(a)

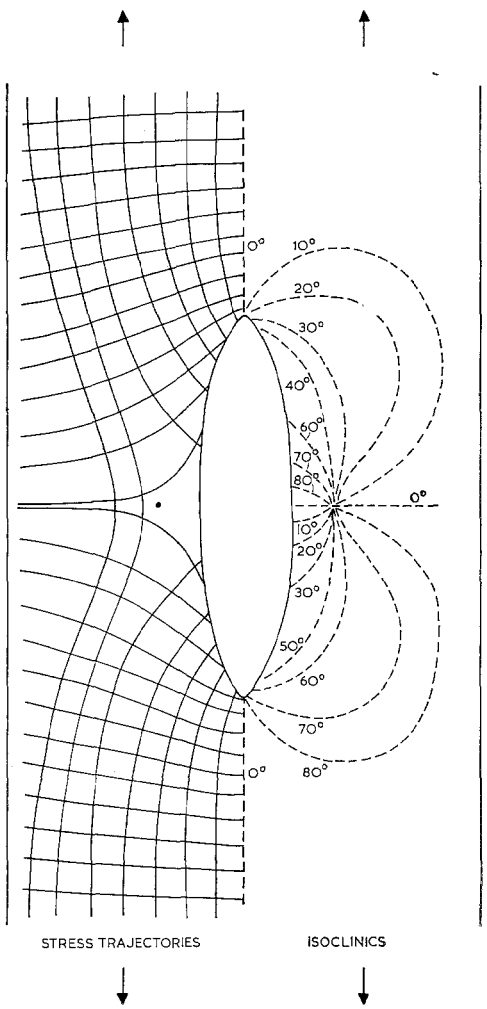

(b)

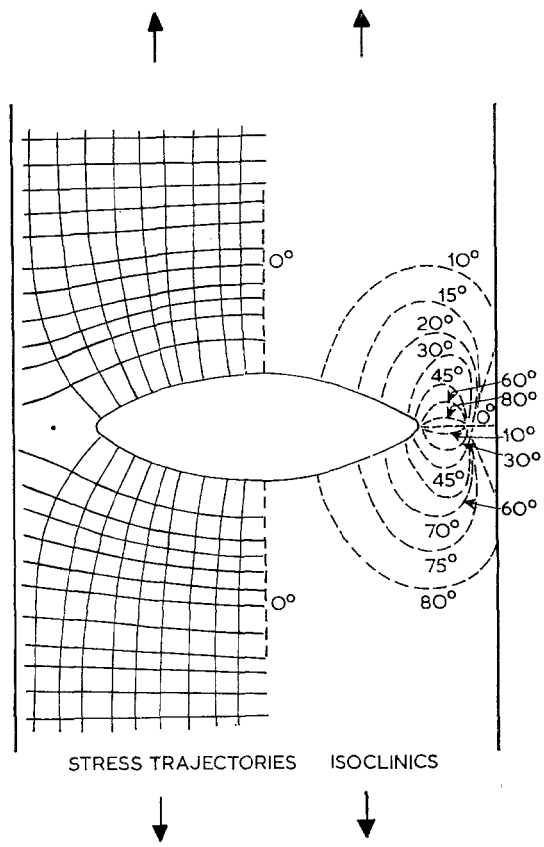

(c)

Figure 2 Isoclinic fringe patterns and stress trajectories in Araldite/brass models: (a) circular inclusion; (b) elliptical inclusion with major axis oriented parallel to applied stress; (c) elliptical inclusion with minor axis oriented parallel to applied stress.

where N is the fringe order, f the material fringe constant, t the model thickness, and $(P - Q)$ the principal stress difference. Frocht's shear-difference method [17] was used to separate the maximum principal stress (P), from the photoelastic data yielding the principal stress difference $(P - Q)$. Fig. 5 shows how the ratio of this stress to the applied stress varies as a function of distance from a circular or elliptical inclusion along the applied stress axis. The curves in figs. 4 and 5 can only be extended to ~ 0.05 cm from the inclusion boundary owing to the difficulty of making accurate experimental observations closer to the inclusion.

Models were made from the photostress plastics, where both matrix and inclusion would

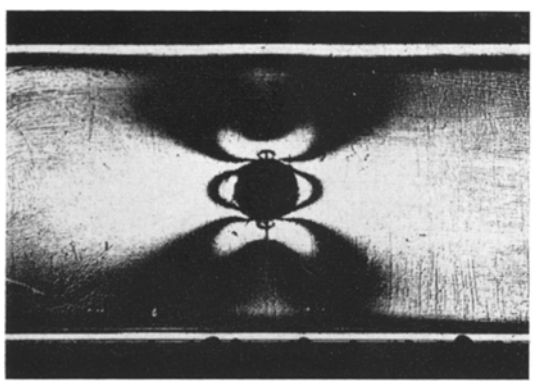

(a)

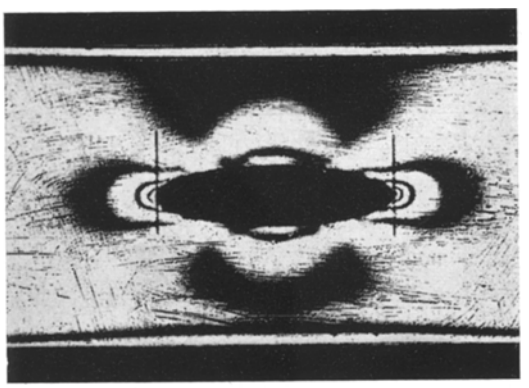

(b)

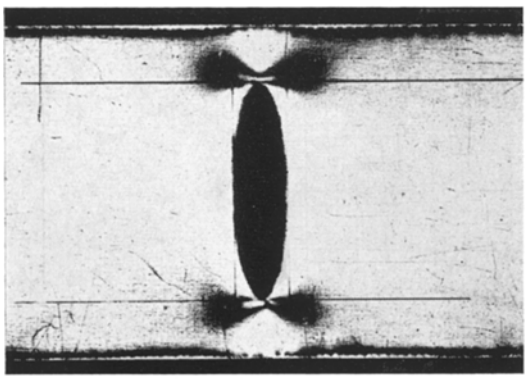

(c)

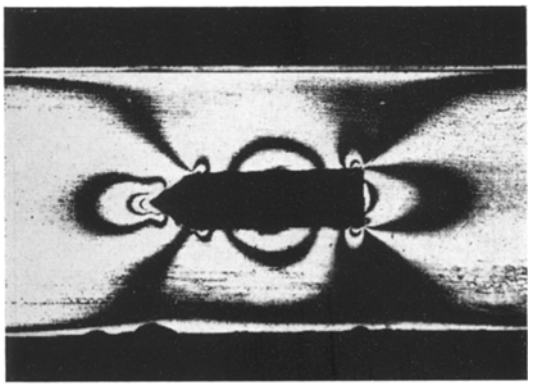

(d)

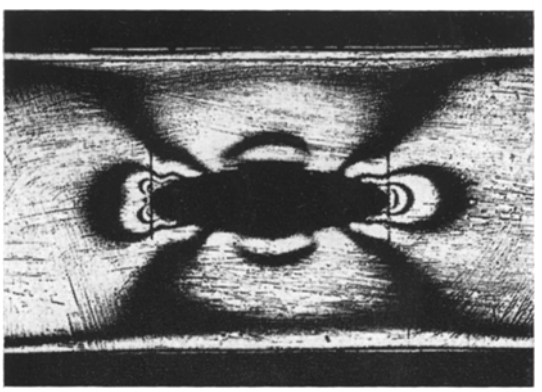

(e)

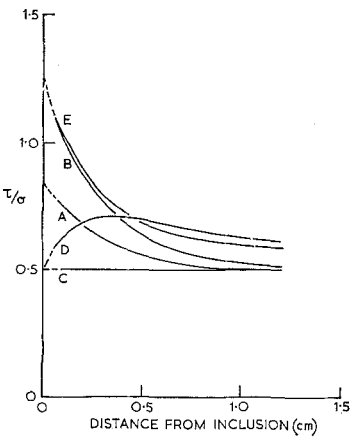

Figure 3 Isochromatic fringe patterns in Araldite/brass models: (a) circular inclusion (3 orders, stress 30 kg/cm^2); (b) elliptical inclusion (4 orders, stress 20 kg/cm^2); (c) elliptical inclusion (2 orders, stress 17 kg/cm^2); (d) irregularly shaped inclusion (3 orders from square end, 5 orders from tapered end, stress 34 kg/cm^2); (e) elliptical inclusion without adhesion at one end (stress 29.5 kg/cm^2).

Figure 4 Ratio of maximum shear stress (τ) to applied normal stress (σ) as a function of distance from inclusion along applied stress axis. A, circular inclusion; B, elliptical inclusion with major axis oriented parallel to applied stress; C, elliptical inclusion with minor axis oriented parallel to applied stress; D, square end of irregularly shaped inclusion; E, tapered end of irregularly shaped inclusion.

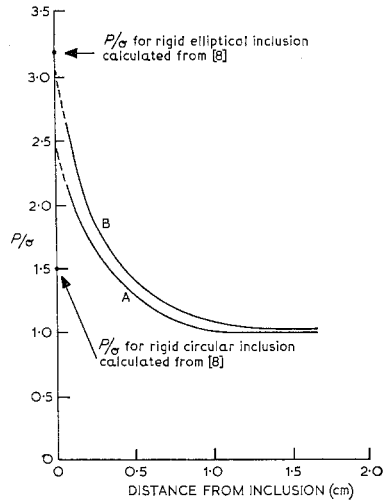

Figure 5 Ratio of maximum principal stress (P) to applied stress (σ) as a function of distance from inclusion along applied stress axis. A, circular inclusion; B, elliptical inclusion with major axis oriented parallel to applied stress.

be photoelastically sensitive, in an attempt to investigate the stress behaviour within the inclusion. The isochromatic fringe patterns obtained for the photostress models are shown in fig. 6. The low modulus Photostress B used for the matrix relaxed rapidly under load and prevented quantitative measurements. However, it was observed that the fringe order within elliptically shaped inclusions was uniform whilst that within irregularly shaped inclusions was non-uniform.

The stress concentrations produced in the matrix at salient points of the boundaries of oblately spheroidal inclusions with both major and minor axes oriented parallel to a uniaxially applied tensile stress were evaluated, using a method due to Eshelby [10]. Eshelby considered an elastically isotropic system of an isolated ellipsoidal inclusion contained by an infinite matrix under stress at infinity. The necessary calculations were carried out using the English Electric KDF9 computer at the University of Birmingham. Fig. 7 illustrates the behaviour of the maximum tensile (positive) and compressive (negative) stress concentrations produced at inclusions (computed stress at point/applied stress), as functions of the axial ratio (a/b) and the ratio (K) of elastic modulus of inclusion to that of the matrix (Poisson's ratio of inclusion and matrix equal to one third). The positions and directions of the computed stresses are shown in the schematic diagrams accompanying fig. 7.

4. Discussion

The photoelasticity technique afforded an immediate demonstration of the existence of stress concentrations at inclusions. The isochromatic fringes (fig. 3) illustrate the perturbation of an otherwise uniform stress field and the likely points of stress concentration, whilst the stress trajectories constructed from the isoclinic fringes (fig. 2) give a qualitative indication of the diffusion of this stress perturbation into the matrix. The experimental technique also allowed observation of the influence of an irregularly shaped inclusion which is difficult to analyse theoretically (fig. 3d).

The number of isochromatic fringes developed

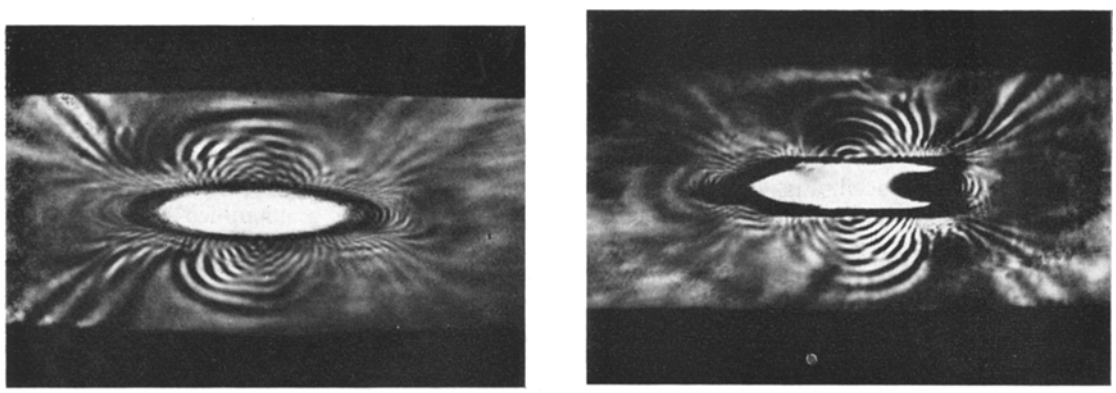

(a) (b)

Figure 6 Isochromatic fringe patterns in photostress models: (a) elliptical inclusion (stress 38.5 kg/cm^2); (b) irregularly shaped inclusion (stress 38 kg/cm^2).

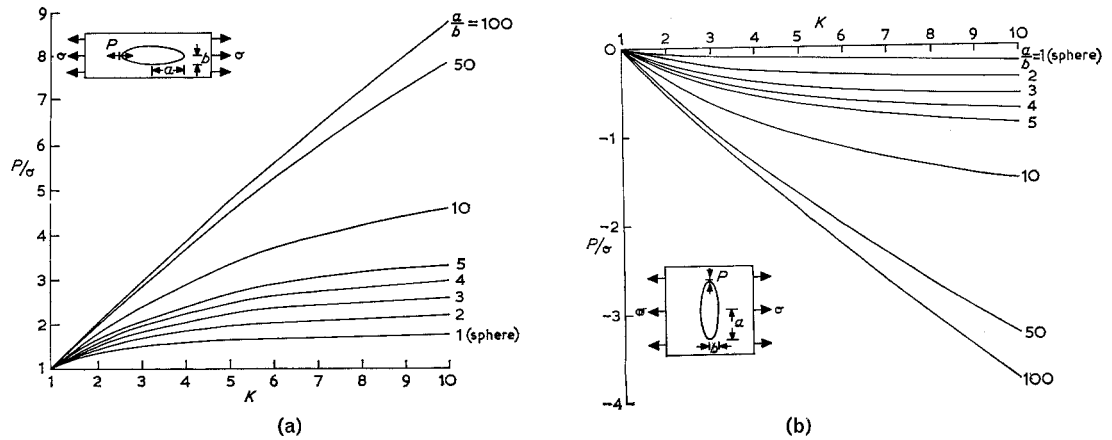

Figure 7 Stress concentration at tips of oblately spheroidal inclusions of various axial ratios (a/b) as a function of the ratio (K) of elastic modulus of inclusion to that of the matrix: (a) major axis oriented parallel to applied stress; (b) minor axis oriented parallel to applied stress.

at a certain point for a particular applied stress also gives a qualitative idea of the stress concentration produced at the point. Thus, the stress at the point where the stress axis cuts the inclusion boundary for an elliptical inclusion with the major axis parallel to the stress axis (fig. 3b) is shown to be greater than that for a circular inclusion (fig. 3a), whilst for an elliptical inclusion with the minor axis parallel to the stress axis (fig. 3c) this stress is about the same as the applied stress. In the latter case the isochromatic fringes concentrate near the tip of the elliptical inclusion, which suggests that this is the source of maximum stress concentration.

It can be seen that acute changes of inclusion shape are the most likely sources of stress concentration. For example, the tapered end of the irregularly shaped inclusion appears to create a stress concentration similar to that of an elliptically shaped end, but greater than that for the square end (fig. 3). These visual observations are supported by actual calculation of the stress concentrations from the photoelastic data. Thus, figs. 4 and 5 give more quantitative evidence of the influence of inclusion shape on the stress concentrations produced. Fig. 4 also illustrates the point of maximum fringe order, and hence of maximum shear stress, at a finite distance from the square end of the irregularly shaped inclusion.

Fig. 5 shows how magnification of the applied stress near the boundary of a circular and elliptical inclusion is reduced with distance from the inclusion along the applied stress axis. In the case of the circular inclusion it can be seen that this stress fall-off is complete at a distance of about $3r$ from the inclusion boundary, where r is the inclusion radius. This is in good agreement with two-dimensional theoretical analysis [6], and with the photoelastic investigation by Thibodeau and Wood [11]. However, the maximum stress concentration produced at a circular inclusion, obtained by extrapolation of the curve in fig. 5, is found to be higher than predicted by theory [6, 8]. On the other hand, the maximum stress concentration produced at an elliptical inclusion is in good agreement with theory [8].

The photostress models showed uniformity of fringe order, and hence of stress, within elliptical inclusions (fig. 6a). This feature has been predicted by Eshelby [10] and used in his treatment of the ellipsoidal inclusion problem. Deviation from the elliptical shape produced non-uniformity of fringe order, and hence of stress, within the inclusion (fig. 6b).

The influence of inclusion modulus, shape and orientation on the maximum stress concentrations produced at inclusions can be further examined by a consideration of the calculated curves in fig. 7. For oblately spheroidal inclusions with their major axis parallel to the applied stress axis a magnified tensile stress is produced at the tip (cf fig. 3b) which increases with increasing axial ratio. For inclusions with the minor axis parallel to the stress axis, a compressive stress is produced at the tip (cf fig. 3c) and this stress is also increased by increasing the axial ratio.

Fig. 7 also shows that an increase in the elastic modulus of the inclusion with respect to that of the matrix always results in an increase

in the stress concentrations produced. It is interesting that, for constant axial ratio, this increase in stress concentration takes place most rapidly during the initial increase of the inclusion modulus above that of the matrix, a point already emphasised for spherical inclusions by Sezawa [6]. For example, the calculated maximum tensile stress produced at the boundary of a spherical inclusion increases to 1.65σ (where σ is the applied stress) for an increase in moduli ratio from 1 to 5, but a further increase in moduli ratio to 10 only increases the stress to 1.75σ. This indicates the possible severity of second-phase inclusions in metallic systems, where the elastic moduli ratio might be expected to lie within this range.

5. Conclusions

(i) The photoelasticity technique enabled an experimental investigation of the stress distribution associated with inclusions in solids.
(ii) The present study demonstrated the possibility of using the photoelasticity technique to determine the stress distribution in and around inclusions of arbitrary shape.
(iii) Local constraint of the matrix by hard inclusions during tensile loading can produce severe stress concentrations.
(iv) The stress concentrations produced depend on the elastic modulus, shape, and orientation of the inclusions.

Acknowledgements

The authors wish to thank Professor G. V. Raynor FRS, for the provision of research facilities and a research studentship for one of them (D.V.E.). They also wish to thank Mr E. Amini of the Department of Mechanical Engineering, University of Birmingham, for the use of photoelastic apparatus, and Dr J. D. Eshelby of the Department of Theory of Materials, University of Sheffield, for helpful discussions.

References

1. J. J. GILMAN, *J. Appl. Phys.* **30** (1959) 1584.
2. J. HOLDEN, *Acta Met.* **8** (1960) 424.
3. F. P. BULLEN, F. HENDERSON, M. M. HUTCHISON, and H. L. WAIN, *Phil. Mag.* **9** (1964) 285.
4. F. P. BULLEN, F. HENDERSON, H. L. WAIN, and M. S. PATERSON, *ibid* p. 803.
5. W. H. MCCARTHY, J. C. SHYNE, and O. D. SHERBY, *Nature* **208** (1965) 579.
6. K. SEZAWA, *Engineering* **135** (1933) 695.
7. J. N. GOODIER, *J. Appl. Mech. Trans. ASME* **55** (1933) A-39.
8. L. H. DONNELL, "Theodore von Kármán Anniversary Volume" (1941) p. 293.
9. R. H. EDWARDS, *J. Appl. Mech.* **18** (1951) 19.
10. J. D. ESHELBY, *Proc. Roy. Soc.* **241** A (1957) 376.
11. W. E. THIBODEAU and L. A. WOOD, *J. Res. Nat. Bur. Stand.* **20** (1938) 393.
12. D. M. SCHUSTER and E. SCALA, *Trans. AIME* **230** (1964) 1635.
13. W. R. TYSON and G. J. DAVIES, *Brit. J. Appl. Phys.* **16** (1965) 199.
14. T. F. MACLAUGHLIN, *Expt. Mech.* **6** (1966) 1.
15. I. M. ALLISON and L. C. HOLLOWAY, *Brit. J. Appl. Phys.* **18** (1967) 979.
16. J. W. DALLY and W. F. RILEY, "Experimental Stress Analysis" (McGraw-Hill, New York, 1965).
17. M. M. FROCHT, "Photoelasticity", Vol. I (Wiley, New York, 1941).